Journal of Applied Electrochemistry **34**: 71–77, 2004.

A photoelectrochemical and spectroscopic investigation of oxide layers on AISI 301 in sulfate solutions at different pH

S. MAFFI[1,*], B. BOZZINI[2], A. FANIGLIULO[2] and L. PERALDO BICELLI[1]
[1]*CESPEL-CNR, Dipartimento di Chimica, Materiali e Ingegneria Chimica "Giulio Natta", Politecnico di Milano, via Mancinelli 7, I-20131 Milano, Italy*
[2]*INFM – Dipartimento di Ingegneria dell'Innovazione, Università di Lecce, via Monteroni, I-73100 Lecce, Italy*
*(*author for correspondence, fax: +39 02 23993180, e-mail: silvia.maffi@polimi.it and luisa.bicelli@polimi.it)*

Received 11 September 2002; accepted in revised form 24 June 2003

Key words: AISI 301, IR spectroscopy, photoelectrochemistry, Raman spectroscopy, stainless steel

Abstract

Photocurrents flowing at AISI 301 stainless steel electrodes, polarized anodically in sulfate solutions of various pH, were related to the nature of the surface oxides formed in these environments. The oxides were identified by surface Raman and IR spectroscopies. Correlations among pH, surface coverage with different types of oxides and photocurrent were recognized by mapping Raman spectroscopy, optical microscopy and image analysis. A high photoresponse is mainly related to high surface coverage with magnetite, formed at high pH. Exposure to low-pH solutions gives rise to preferential formation of hematite. Magnetite formed at high pH is irreversibly transformed into hematite if the oxide layer is subsequently exposed to a low-pH solution.

1. Introduction

AISI 301 is an austenitic stainless steel with low Cr and Ni contents. It provides a good balance of mechanical and corrosion resistance for a convenient price. The low Cr and Ni contents give rise to improved work hardenability, but limited corrosion performance. It is commonly used in applications where a stainless steel is needed, but the chemical environment is not so harsh as to require high corrosion resistance standards. Typical applications are in tubing for single-phase aqueous process flows. Erosion–corrosion even with moderate flow regimes proved to be a drawback for the application of this material in some instances. The mechanical stability of the oxide surfaces, particularly the uppermost surface, in contact with the flowing solution is vital for erosion–corrosion performance. It is, therefore, critical to gain insight into the nature of these films as a function of exposure conditions.

In this paper we relate photoelectrochemical (PEC) measurements with surface spectroscopic measurements, in order to characterize the uppermost oxide layers grown onto AISI 301. Since the photocurrent derives from the layer which is photoactive under the given excitation wavelengths, we employed a Xenon arc lamp (light power density 50 mW cm^{-2}) with a wide wavelength range able to excite the Fe oxides (magnetite, band gap (b.g.) 1.65 eV, hematite b.g. 1.9 eV) as well as the Cr and Ni oxides (b.g. ~3.5 eV), although the latter two are close to the low wavelength limit of the lamp emission. However, since we performed anodic measurements, the PEC response is from the n-type Fe oxides rather than from the p-type Cr or Ni ones. The Fe-rich uppermost, thicker, oxide layer, only, is therefore expected to yield a photocurrent in our experimental conditions. Surface vibrational spectroscopies, such as IR and Raman, are suitable for the characterization of the uppermost, photoactive part of the oxide film.

A limited amount of work is available on the anodic electrochemical behaviour of AISI 301 [1]. Most corrosion studies on this type of stainless steel are based on potentiodynamic measurements and stress their environmental performance as a function of metallurgical conditions, in particular the degree of cold working. No specific studies are available on the oxide layer structures and compositions of AISI 301, to the best of the authors' knowledge.

Auger electron spectroscopy (AES) and X-ray photoelectrons spectroscopy (XPS) studies of other austenitic stainless steels have shown that the Cr-content of the uppermost layer increases as the passivation potential is approached [2–7]. This Cr-enrichment is believed to be due to selective dissolution of Fe from the oxides. Duplex and triplex layer structures were identified: the inner layers are rich in Cr, the outer layer is Fe-rich and tends to contain hydroxide or bound water [7, 8]. Mixed Fe and Ni oxides have also been reported for the outer layer [9] grown on AISI 316L.

2. Experimental details

2.1. *Materials*

50 μm thick foils of AISI 301 stainless steel, provided by Sandvick, were used. Their composition was verified by quantometry and resulted to be C 0.1%, Si 1.2%, Mn 1.3%, Cr 16.5%, Ni 7.5%, Mo 0.7%. Samples of dimensions 2 cm × 2 cm were tested in aerated solutions at the following pH values: 1.7, 2, 4, 4.6, 6.5, 6.9, 9.2, 11, 13. Solutions at various pH were obtained by mixing suitable amounts of sulfuric acid and sodium hydroxide. PEC measurements were carried out in the above-mentioned solutions at various pH values. Electrochemical measurements were carried out in 1 M sodium hydroxide.

2.2. *Electrochemical measurements*

Potentiodynamic and potentiostatic measurements were performed with a three-electrode configuration in a prismatic cell containing 300 ml of aerated solution. A computer-controlled potentiostat was used. The counter electrode was a platinized titanium expanded mesh electrode. The reference electrode was silver | silver chloride (0.222 mV vs NHE). All voltages, are reported on the normal hydrogen electrode (NHE) scale.

Before electrochemical measurements a cathodic pretreatment was applied in an attempt to provide a reproducible starting condition prior to anodic polarization and related oxide growth. The procedure and its physico-chemical meaning in terms of chemical actions on preexisting oxides and modifications induced by hydrogen evolution are not well established and actually need further investigation; nevertheless this approach is commonly applied with the aim of reducing oxide films or to evaluate film thicknesses [10] and does produce empirically reproducible electrochemical conditions.

2.3. *Photoelectrochemical measurements*

For PEC measurements a conventional three-electrode cell was used. The incident light was focused on the working electrode through a quartz window. The reference electrode was a saturated calomel electrode whereas the counter electrode was a platinum wire.

Before the experiments, the samples of AISI 301 stainless steel were degreased in carbon tetrachloride and no other treatment was performed. The samples surface in contact with the electrolyte was 2 cm^2.

A 150 W xenon lamp (Oriel) was used as the light source and the light was chopped at a frequency of 24 Hz. The photocurrent was measured with a lock-in amplifier (5610B/A NF Electronic Instruments).

2.4. *Surface Raman spectroscopy*

Surface-enhanced Raman Spectroscopy (SERS) measurements were carried out with a MicroLabRam confocal Raman system. Excitation at 632.8 nm is provided by a 12 mW He–Ne laser. A 10× objective was used. The lateral resolution of the system is 0.5 μm. The reported Raman intensities are directly proportional to the discharge current of the CCD element corresponding to a given frequency, uncorrected for the quantum efficiency.

2.5. *FTIR reflection absorption spectroscopy*

FTIR reflection absorption spectroscopy (FTIRRAS) measurements were carried out with a Nicolet NEXUS. A Harrick VRA variable-angle external-reflection variable-angle reflection device was employed. The resolution was set to 2 cm^{-1}. The number of spectra accumulations was 32. Spectra were acquired in the single-beam mode.

2.6. *Optical microscopy and image analysis*

Optical microscopy was carried out with a Nikon Epiphot 200, quantitative image analysis was performed with the 'Lucia' software. The optimal magnification was 500×. Image treatment was performed with the following parameters: contrast 74/255, brightness 125/255, dimension: 279 × 203 μm^2. The black/white ratio was computed on two-colour images obtained from original ones after assignment of white colour to pixels having a grey tone higher than a suitable threshold value. The optimal threshold level (60/255) was established by varying it until shadows from bright areas (brought about by the presence of lamination lines on the samples) were assigned to the white channel and thin chain-fashioned dark oxides fell into the black channel.

3. Results and discussion

3.1. *Electrochemical measurements*

Potentiodynamic measurements were carried out in order to characterize the anodic behaviour of the material under the electrochemical conditions adopted during the PEC measurements. The sample was polarized cathodically at −2.3 V for 30 min in 1 M sodium hydroxide, then the sample was left at open circuit for 3 min, after which an anodic scan was imposed from open circuit to +1700 mV with a scan rate of 2 mV s^{-1}. The polarization curve (Figure 1) displays two plateau regions followed by a Tafel-type rise at a potential higher than the equilibrium oxygen evolution potential. Under these electrochemical conditions a passivation peak could not be observed, the first anodic plateau (−80 to 120 mV) is due to the oxidation of some ill-defined reduction product formed during the cathodic pretreatment. A full identification of these species is beyond the scope of this paper, since in this context we are chiefly interested in achieving a highly reproducible potentiodynamic behaviour and this aim cannot be

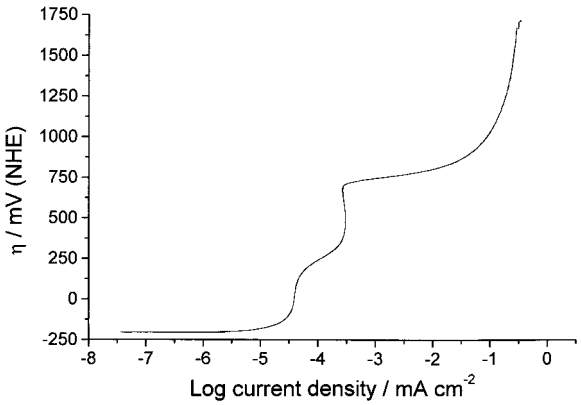

Fig. 1. Polarization curve of AISI 301 in 1 M NaOH; anodic scan from open circuit to +1700 mV with a scan rate of 2 mV s^{-1}.

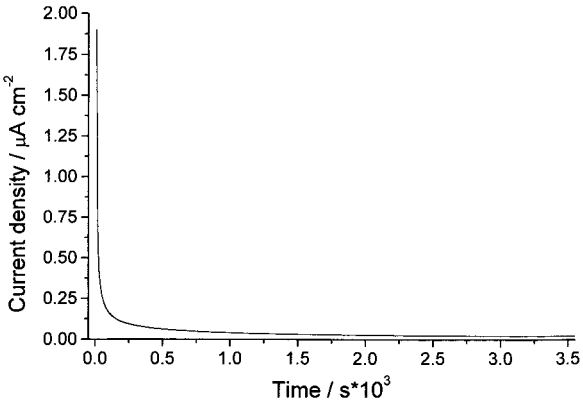

Fig. 2. Current relaxation transient measured at potentials within the plateau range from +320 to +720 mV.

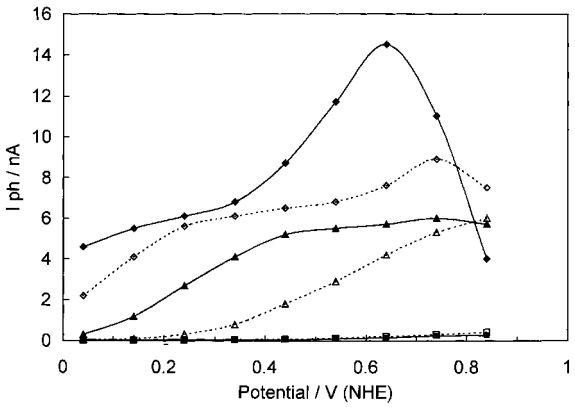

Fig. 3. Photocurrent measurements for AISI 301 in sulfate solutions at different pH. Key: (♦) 13.0, (◇) 11.0, (▲) 9.2, (△) 6.9, (■) 4.6 and (□) 1.7.

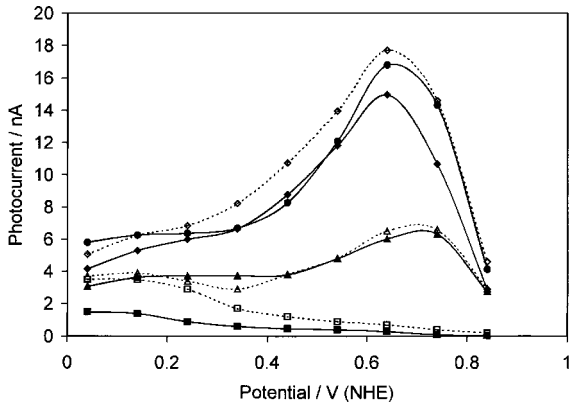

Fig. 4. Photocurrent measurements in NaOH solution at pH 13 for AISI 301 previously treated by immersion in sulfate solutions at different pH. Key: (●) 13, (♦) 6.5, (◇) 6.5*, (▲) 4, (△) 4*, (■) 2 and (□) 2* measurement repeated after one day.

fulfilled without some kind of pretreatment such as that proposed in this work. The second anodic plateau (+320 to +720 mV) is possibly related to passivity conditions. Current relaxation transients after the same prepolarization procedure were measured at potentials within the second plateau range. A rapid decay of the anodic current (again, possibly related to hydrogen oxidation) is observed, followed by a slow relaxation settling down at very low current densities (a few nA cm^{-2}). A typical transient (at +470 mV) is shown in Figure 2.

3.2. *Photoelectrochemical measurements*

Photocurrent measurements were performed by polarizing the samples in the range +40 to +840 mV. As far as the environments are concerned, two series of experiments were considered. In the first one the sample was immersed in the sulfate solutions at different pH and the PEC measurements were carried out after 20 min. In the second one the sample was alternatively immersed in a solution of pH 13 and in a solution of lower pH for 20 min. The pH values were 6.5, 4, and 2. The PEC measurements were always carried out in the solution at pH 13 after a preliminar anodic polarization of the sample at +640 mV for 15 min. Then, the electrode was polarized again at +640 mV for at least one day before repeating the measurement. After this treatment the sample was immersed in a solution at a lower pH and a new test was started.

The results are reported in Figures 3 and 4, respectively. The trends of the curves are extremely reproducible. Photocurrent values are typically correlated with pH. By comparing Figures 3 and 4 it can be concluded that the main effect on photocurrents is related to the lowest pH at which the samples have been exposed. This is reasonably related to the formation of stable and different oxide layers in the solutions at different pH. In addition to the gross differences in photoresponse related to pH, a growing trend of the photocurrent as a function of potential can also be noticed. This growing trend might be related to the fact that photoactive Fe(III)-rich oxides are progressively stabilized at increasingly anodic potentials. The photocurrent vs. potential plots show two approximately linear regions with two slopes: a less steep slope for potentials below about +220 mV and a steeper slope for potentials above about +320 mV. These two ranges can be straightforwardly related to the potentiodynamic curve reported in

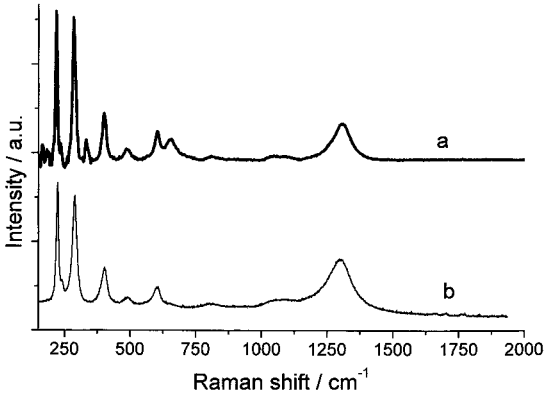

Fig. 5. (a) Raman spectrum of sample at pH 1. (b) Raman spectrum of hematite.

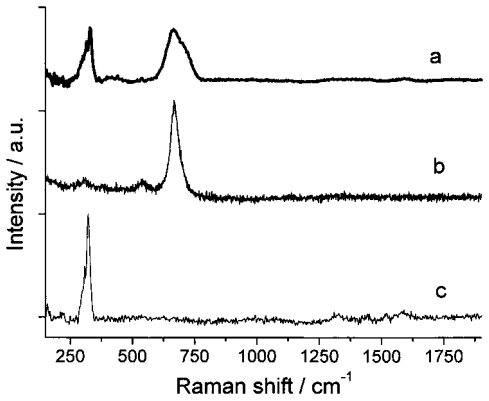

Fig. 6. (a) Raman spectrum of sample at pH 7. (b) Raman spectrum of magnetite. (c) Raman spectrum of nickel oxide.

Figure 1, with the lower slope corresponding to preplateau conditions, while the steeper slope relating to passive conditions. Measurements at potentials higher than 620 mV display lower photocurrents, possibly also owing to anodic alterations brought about by transpassive behaviour or oxygen evolution.

3.3. *Surface Raman spectroscopy*

Raman spectra were measured for samples immersed in solutions at several pH values for 3 days at room temperature at the free corrosion potential. Raman spectra were measured for the following standards: hematite (α-Fe_2O_3), magnetite (Fe_3O_4), $FeSO_4$, NiO, Cr_2O_3. Band assignment was performed by comparison between the AISI 301 samples and these standards.

The Raman spectra of all the samples show two types of band pattern: (i) mainly hematite, with traces of magnetite and NiO (Figure 5), (ii) mainly magnetite and NiO, with traces of hematite (Figure 6). These band patters are related in a simple way to the appearance of the samples treated in solutions of different pH. The samples surfaces present dark and bright spots which could be analysed separately thanks to the imaging and confocal facilities of the MicroLabRam spectrometer: dark spots show type (i) bands, bright ones type (ii)

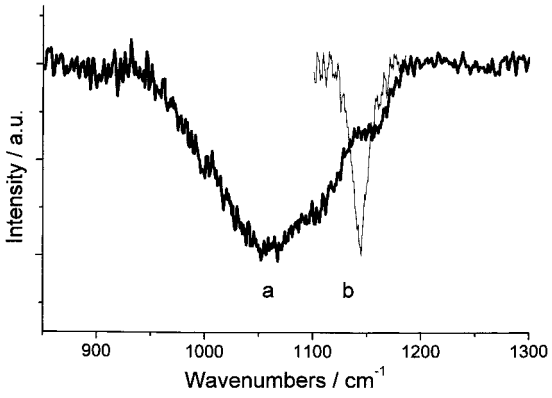

Fig. 7. FTIR spectra at pH < 5 (a) and pH 6.5 (b) after background subtraction and an FFT smoothing with 25 points.

bands. Type (i) bands dominate low-pH samples, type (ii) bands dominate for pH values higher than 6.9. The simultaneous presence of magnetite and NiO might be indicative of the presence of mixed Fe–Ni oxides, such as the spinels reported in [9] for AISI 316L. Peaks related to Cr-oxides could not be observed in our spectra. This result is expected from the literature on duplex and triplex oxide layers on stainless steels, implying that Cr is typically present in the innermost layers, and from the fact that the Raman signal in our system cannot derive from oxide thicknesses in excess of that of the Fe-rich uppermost layers grown in these conditions [9, 11].

3.4. *FTIR reflection–absorption spectroscopy*

FTIRRAS was used to discriminate between surface oxides and hydroxides. Samples prepared at pH 1.7 and 4.6 display a broad band at 1050 cm^{-1}, which is typical for Fe(III)-oxyhydroxide (δ-FeOOH) [12–14], while samples grown at higher pH show a narrow peak to 1145 cm^{-1}, which is typical for Ni(II)-hydroxide (β-$Ni(OH)_2$) [15, 16] (Figure 7). The fact that the δ-FeOOH peak dominates the IR spectrum is compatible with the fact that hematite is the dominating surface species at pH 1.7 and 4.6. A similar observation holds regarding the dominance of the β-$Ni(OH)_2$ peak in the IR spectra at higher pH and the corresponding simultaneous dominance of magnetite and NiO measured in the Raman spectra.

3.5. *Optical microscopy and image analysis*

As far as the visual appearance of the attacked surfaces is concerned, samples immersed in solutions at pH 1.7 and 4.6 appear fully covered with a dark film, while the samples treated in solutions at higher pH show some dark spots, but essentially show a bright appearance. Optical microscopy (OM) observations disclose that the actual microscopic morphology is the same at all pH values and consists of dark and bright areas of the same aspect, the relative amounts of dark and bright spots vary regularly with pH. The relative amounts of the two

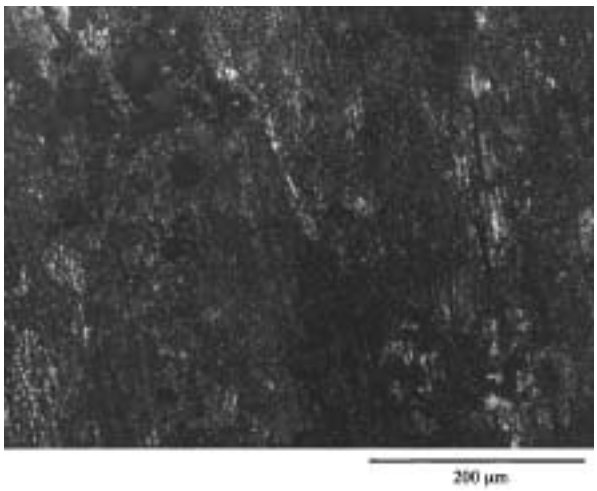

Fig. 8. Photograph taken on sample at pH 1.

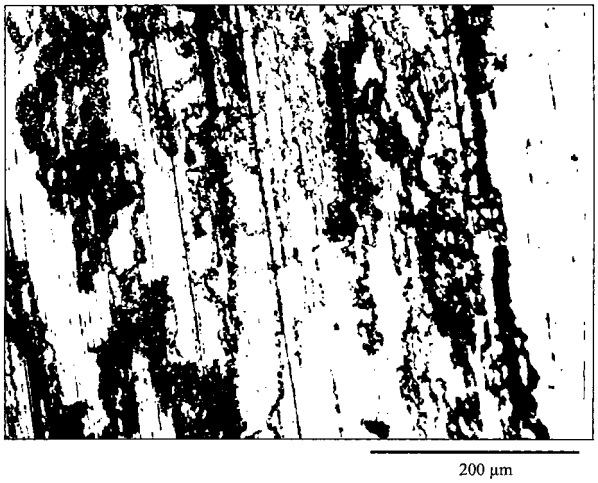

Fig. 10. Black–white image obtained from photo at pH 11 (previous Figure), threshold level 60/255.

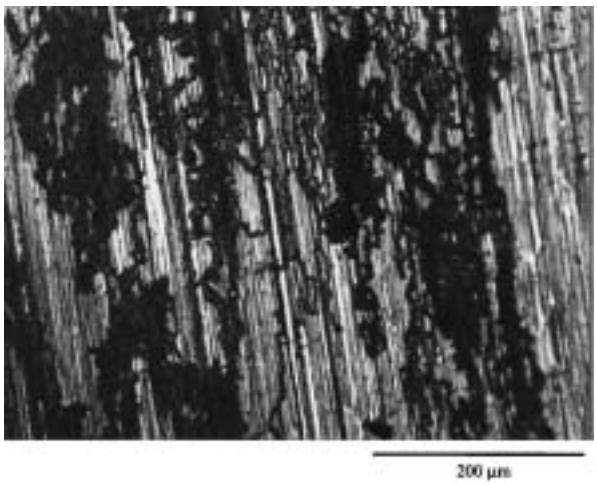

Fig. 9. Photograph taken on sample at pH 11.

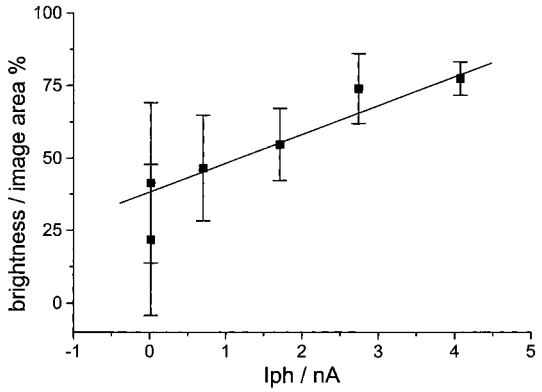

Fig. 11. Estimation of the correlation between the average brightness of an image and the average photocurrent in the passivity range of the corresponding sample for each pH value; linear fit gave $\rho = 0.94784$ and $\sigma = 0.4919$.

types of material were quantified by image analysis (the relevant procedure is described in Section 2.6) in an attempt to correlate the surface coverage with the chemical nature of the two types of spots and to the corresponding PEC behaviour. The average brightness, estimated by image analysis of 500× OM pictures (Figures 8–10), was correlated to the pH at which the surfaces were treated and to the average photocurrent values in the passivity range (+320 to +720 mV) recorded at the respective pH (Figure 11).

3.6. *General discussion*

In addition to the electrochemical oxidation processes, PEC reactions take place on the film surface due to oxidation of redox systems present in the electrolyte, mainly the water redox couples. At rest conditions the passive film will behave as a mixed electrode with a redox potential intermediate between that of the H_2/H^+ and OH^-/O_2 redox systems, but closer to the latter, since oxygen is present in our solutions. The onset potential of the photocurrent is related to the flatband potential of the metal oxides which depends on the electrolyte pH because of the additional potential drop across the Helmholtz double layer due to specific surface adsorption of H^+ or OH^- ions in acidic or alkaline solutions, respectively. The theoretical (thermodynamic) pH dependence is the same as that of the hydrogen and oxygen redox couples. Therefore, a shift of the onset potential is expected towards more anodic values with decreasing pH, as experimentally observed. As to the main oxides formed at different pH and to their PEC behaviour, Raman spectra show the presence of Fe_3O_4 and NiO at the highest pH and of Fe_2O_3 at the lowest pH.

The theoretical flatband potentials of the two iron oxides, assuming there is no net charge across the Helmholtz double layer other than the small dipole contribution of the solvent, that is, at the pH of the point of zero zeta potential (pzzc) [17–21], E_{FB}(pzzc), are expected to be practically the same. Indeed, the electronegativity, χ, of the two oxides (determined from that of their constituent atoms) and the band gap, E_g, from which E_{FB}(pzzc) may be evaluated, are very close, as shown in Table 1. The procedure for the computation

Table 1. Electronegativity, band gap, point of zero zeta potential and flatband potential at different pH for several metal oxides

Oxide	χ /eV [17]	E_g /eV [23]	pzzp(pH)	E_{FB}(pzzp) /V vs NHE	E_{FB}(pH 1.68) /V vs NHE	E_{FB}(pH 13) /V vs NHE
n-Fe_2O_3	5.88	1.9	8.6 [18]	0.69	1.09	0.43
n-Fe_3O_4	5.77	1.65	6.5 [19]	0.70		0.32
p-NiO	5.74	3.5	10.3 [20]	2.85		2.69
p-Cr_2O_3	5.66	3.5	8.1 [21]	2.77		2.48

of the semiconductor film quantities reported in Table 1 is described in [22]. Band gap values were derived from the literature [23]. In these calculations, we assumed the difference between the conduction band edge and the flatband potential at the surface, $E_c - E_{FB}$, for the n-type oxides to be −0.2 eV, as usual for oxides having a low to medium donor concentration. Similarly for the difference between the flatband potential at the surface and the valence band edge, $E_{FB} - E_v$, for p-type oxides. We preferred to determine the flatband potential theoretically instead of using published experimental values as they are largely dispersed because of the different preparation conditions of the bulk oxides and of the different compositions of iron alloys where the oxides are present. NiO and Cr_2O_3 are both p-type and have electronegativity values close to those of the two iron oxides. As expected, they have a much higher E_{FB}(pzzc) because of their much higher band gap (Table 1). The flatband potentials recalculated at the actual pH of the solutions, i.e., at pH 1.68 that of Fe_2O_3 and at pH 13 those of Fe_3O_4, NiO and Cr_2O_3 are also reported in Table 1. The high value of the Fe_2O_3 flatband potential and the much lower value of that of Fe_3O_4 are in agreement with the trend of the onset potentials of the experimentally determined curves. In particular, the strong photocurrent increase observed at about +0.350 V of the pH 13 curve matches the value of the flatband potential of Fe_3O_4. As expected, the PEC photoresponse of NiO and of Cr_2O_3 can not be detected in our experimental conditions.

It is worth noting that very accurate E_{FB} values have been measured for cognate systems (AISI 304 and 316 in borate buffer solutions) [24]. Our estimated values are significantly higher than those reported in this reference. Nevertheless the differences in materials, polarization procedure and evaluation method (we used an indirect numerical procedure while the data of [24] were obtained by direct measurement) explain this inconsistency. Possible inaccuracies in our estimate of E_{FB} would not impair the relative and ranking use we are making of these values.

Notwithstanding the simplifications of the treatment, which has not considered the complex nature of the passivating films regarding their real composition, structure, defect concentration etc., this approach is able to give a general interpretation of the observed phenomenology. In conclusion, the PEC curves as a function of the exposure conditions reflect the pH dependence of the flatband potentials of metal oxides, that is their shift towards more anodic values decreasing the pH. As far as the curves reported in Figure 4 are concerned, they are all measured in the same electrolyte at pH 13 after a short treatment in solutions of decreasing pH. For pH higher than 2, the trend of the curves is the same although lower photocurrents are observed. For pH 2, the trend is different, and a vanishing photoresponse is obtained. The Fe_2O_3 film formed at pH 2 can obviously not be reduced by anodic treatment to Fe_3O_4, to which the high photocurrents may be ascribed. Moreover, the very low photocurrents also seem to indicate a permanent modification of Fe_2O_3, possibly due to the formation of iron hydroxides.

4. Conclusions

From a combination of photoelectrochemical, electrochemical and surface vibrational spectroscopic results, it can be concluded that the pH of solutions at which AISI 301 stainless steel surfaces are exposed brings about variations of the relative amounts of Fe-rich oxides. Exposure to low pH solutions gives rise to the formation of larger amounts of hematite; apparently magnetite (which tends to be preferentially formed at higher pH) is converted into hematite by exposure to low-pH solutions. This change is of course irreversible with respect to pH changes.

Surface morphologies observed by optical microscopy can be straightforwardly related to Raman band patterns, thus allowing discrimination between areas in which hematite or magnetite are the dominating forms of Fe-rich oxide. Quantitative relations can be drawn between surface coverage with hematite and photocurrent.

From a technological point of view, it is interesting to observe that the exposure of this material to low-pH solutions, even for comparatively limited amounts of time (e.g., acid cleaning in a plant where neutral or alkaline solutions are typically handled), is liable to lead to a variation of the nature of the uppermost oxide layers which might lead to dramatic changes in functional behaviour of the material. In particular, as far as erosion–corrosion performance is concerned, it is known that the mechanical stability of the oxide surfaces on stainless steel is related to the relative content of the type of oxide, magnetite being more stable than hematite. Photoelectrochemical measure-

ments can provide a rapid and accurate (possibly *in situ*) estimate of changes undergone by the surface oxides.

References

1. A. Barbucci, M. Delucchi, M. Panizza, M. Sacco and G. Cerisola, *J. Alloy Comp*. **607** (2001) 317–318.
2. G. Okamoto, *Corros. Sci.* **13** (1973) 471.
3. I. Olefjord and H. Fischermeister, *Corros. Sci.* **15** (1975) 697.
4. K. Asami, K. Hashimoto and S. Shimodaira, *Corros. Sci.* **16** (1976) 387.
5. K. Asami, K. Hashimoto and S. Shimodaira, *Corros. Sci.* **18** (1978) 125.
6. C. Laygraf, G. Hulqvist, I. Olefjord, B.O. Elfström, V.M. Knyazheva, A.V. Plaskeyev and Y.M. Kolotyrkin, *Corros. Sci.* **19** (1979) 343.
7. K. Asami, K. Hashimoto and S. Shimodaira, *Corros. Sci.* **17** (1977) 713.
8. J.E. Castle and C.R. Clayton, *Corros. Sci.* **17** (1977) 7.
9. M. da Cunha Belo, M. Walls, N.E. Hakiki, J. Corset, E. Picquenard, G. Sagon and D. Noël, *Corros. Sci.* **40** (1998) 447.
10. J.E.O. Mayne and P. Ridgewa, *Br. Corros. J.* **6** (1971) 244.
11. P. Schmutz and D. Landolt, *Corros. Sci.* **14** (1999) 2143.
12. W. Tschinkel, H.Neugebauer and A. Neckel, *J. Electrochem. Soc.* **137** (1990) 1475.
13. B. Pal and M. Sharon, *Thin Solid Films* **379** (2000) 83.
14. S. Nasrazadani, *Corros. Sci.* **39** (1997) 1845.
15. B. Beden and A. Bewick, *Electrochim. Acta* **33** (1988) 1695.
16. J. Desilvestro, D.A. Corrigan and M.J. Weaver, *J. Electrochem. Soc.* **135** (1988) 885.
17. M.A. Butler and D.S. Ginley, *J. Electrochem. Soc.* **125** (1978) 228.
18. R.J. Arkinson, A.M. Posner and J.P. Quirk, *J. Phys. Chem.* **71** (1967) 550.
19. I. Iwasaki, S.R.B. Cooke and Y.S. Kim, *Trans. AIME* **223** (1962) 113.
20. G.A. Park, *Chem. Rev.* **65** (1965) 177.
21. K. Emerson and W.M. Gravea, *J. Inorg. Nuclear Chem.* **11** (1959) 309.
22. L. Peraldo Bicelli, *J. Phys. Chem.* **96** (1992) 9995.
23. F. Di Quarto, C. Sunseri, S. Piazza and M.C. Romano, *J. Phys. Chem. B* **101** (1997) 2519.
24. N.E. Hakiki, M. Da Cunha Belo, A.M.P. Simões and M.G.S. Ferreira, *J. Electrochem. Soc.* **145** (1998) 3821.